Rare Met. (2018) 37(8):642–649
https://doi.org/10.1007/s12598-017-0926-5
RARE METALS
www.editorialmanager.com/rmet

Microstructure and thermoelectric properties of $Bi_{1.9}Lu_{0.1}Te_3$ compound

Maxim Yaprintsev, Roman Lyubushkin, Oxana Soklakova, Oleg Ivanov*

Received: 3 October 2016 / Revised: 8 February 2017 / Accepted: 11 May 2017 / Published online: 26 July 2017

Abstract Effect of fabrication conditions on microstructure and thermoelectric properties of the $Bi_{1.9}Lu_{0.1}Te_3$ compound was studied. Starting nanopowder with mean nanoparticle size of ~37 nm was synthesized by a microwave–solvothermal method. In order to prepare samples with various micro-grained structures, the synthesized nanopowder was compacted by two methods. The first method is cold isostatic pressing with further high-temperature annealing, while the second method is spark plasma sintering at various temperatures of process (653 and 683 K). It is found that mean grain size is equal to ~290, ~730 and ~1160 nm for cold isostatically pressed and spark plasma sintered at 653 and 683 K samples, respectively. The micro-grained sample with maximum mean grain size shows the best thermoelectric properties. This sample is structurally inhomogeneous and has the lowest thermal conductivity and the specific electrical resistivity. Maximum dimensionless figure of merit for this sample is equal to ~0.9 for temperature range of 450–500 K.

Keywords $Bi_{1.9}Lu_{0.1}Te_3$ compound; Spark plasma sintering; Cold isostatic pressing; Grain structure; Thermoelectric properties

M. Yaprintsev, R. Lyubushkin, O. Soklakova, O. Ivanov*
Joint Research Centre, Belgorod State University, Belgorod, Russian Federation 308015
e-mail: OlegIvanov@bsu.edu.ru

O. Ivanov
Voronezh State Technical University, Voronezh, Russian Federation 394026

1 Introduction

At present, bismuth telluride, Bi_2Te_3 and Bi_2Te_3-based compounds are known as the best low-temperature thermoelectric materials [1–3]. Efficiency of thermoelectric materials is characterized by the thermoelectric figure of merit (ZT). The dimensionless figure of merit is defined as $(S^2\gamma/k)T$, where T is the absolute temperature, S is the Seebeck coefficient, γ is the electrical conductivity, and k is the total thermal conductivity with contributions from the lattice and the charge carriers [4]. The ZT value of the commercial Bi_2Te_3-based compounds has remained around 1 for many years. A number of investigations have focused on optimizing the composition, tuning doping with other heavy metals, fabricating the various nanostructures, etc., in order to improve thermoelectric properties of the Bi_2Te_3-based materials [5–8]. Recently, it has been found that doping Bi_2Te_3 with rare earth elements (Lu, Ce, Sm, Er, La, etc.) can also improve thermoelectric properties of Bi_2Te_3-based materials [9–16].

According to Ref. [9], rare earth element doping has several effects on the thermoelectric properties of Bi_2Te_3 compound. Firstly, atoms of rare earth elements substituting for Bi site in the Bi_2Te_3 compound behave as donors and increase the carrier concentration which is beneficial for the reduction of the electrical resistivity but is harmful to the Seebeck coefficient. Then, using rare earth atoms to replace bismuth atoms will lead to further alloying which can additionally scatter both charge carriers and phonons. Additional scattering of phonons will reduce thermal conductivity. On the one hand, additional scattering of charge carriers can increase the scattering factor and enhance the Seebeck coefficient. On the other hand, scattering of charge carriers can increase the electrical resistivity through reducing the average relaxation time of the charge carriers.

Finally, the thermal conductivity of the rare earth containing Bi_2Te_3-based compounds is usually higher than the thermal conductivity of the undoped Bi_2Te_3. Actually, the mass of rare earth atoms is less than that of bismuth atom. In this case, the frequency of phonons should be increased as heavy bismuth atoms are replaced with lighter rare earth atoms. However, the lutetium atom mass is very close to the bismuth atom mass as compared with other rare earth atoms. So, Lu-doping can avoid sufficient increase of the phonon frequency and remain the low thermal conductivity of Bi_2Te_3. Thus, in order to improve the thermoelectric properties of the Bi_2Te_3 compound, lutetium doping will be more effective than other rare earth elements.

Important parameter influencing thermoelectric properties of the thermoelectric is a grain structure [17–21]. It is known that both grain size and grain size distribution are key structure parameters of the micro- and nano-grained thermoelectric materials by controlling their electrical and thermal properties [22–27]. In order to form a desired microstructure, various methods of thermoelectric materials fabrication including preparation of the starting powder, compacting the starting powder and high-temperature treatments should be used. The aim of this paper is to study the effect of fabrication conditions on grain structure and thermoelectric properties of $Bi_{1.9}Lu_{0.1}Te_3$ compound.

2 Experimental

Microwave–solvothermal synthesis was applied to prepare the starting $Bi_{1.9}Lu_{0.1}Te_3$ powder. As known, compared with the conventional methods, the microwave-assisted heating technique has the advantages of very short time of synthesis, simplicity and energy efficiency, small particle size of the products, narrow particle size distribution and high purity [28, 29]. Analytically pure chemicals were used for the synthesis (bismuth oxide, Bi_2O_3, tellurium oxide, TeO_2, lutetium oxide, Lu_2O_3, ethylene glycol, nitric acid and *N*,*N*-dimethylformamide).

The Bi_2O_3, TeO_2 and Lu_2O_3 oxides taken in a stoichiometric ratio were dissolving in mixture of concentrated nitric acid and ethylene glycol. Then, *N*,*N*-dimethylformamide was added in mixture after dissolving. The microwave-assisted reaction was carried out in a MARS-6 microwave reactor, with a power of 1000 W at a working frequency of 2.45 MHz. The synthesis was carried out for 15 min at temperature of 463 K and pressure of 4 MPa.

Two sintering methods were used to form various grain structures of bulk $Bi_{1.9}Lu_{0.1}Te_3$ materials. According to the first method, the powder after synthesis was cold isostatically pressed (CIP) at 250 MPa by using an EPSI cold isostatic press. Pressed samples were then sintered at 683 K for 2 h at Ar atmosphere. Spark plasma sintering (SPS) method was applied as the second method by using a SPS-25/10 system. Two temperatures of 653 and 683 K of the SPS process were used. These SPS temperatures allowed forming a quite different grain structure of the bulk material. Pressure and time of the SPS process were, respectively, 40 MPa and 5 min for both SPS temperatures.

Phase compositions of the starting powder and the bulk materials were determined by X-ray diffractometer (XRD, Rigaku Ultima IV) with Cu Kα radiation. Particles size and morphology of the starting powder were examined by using a transmission electron microscope (TEM, JEM-2100). Scanning electron microscope (SEM, Nova NanoSEM 450) was used to study the microstructure of the bulk samples prepared. The specific electrical resistivity and the Seebeck coefficient were measured using a ZEM-3 system. A TC-1200 system was applied to determine the thermal conductivity by the laser flash method.

Measurement by the laser flash method was used to find thermal diffusivity. This method examines the temperature change with time of the back side of a sample after heating the front side with laser beam instantaneously. The thermal conductivity (k) of a sample is found from thermal diffusivity (α), the specific heat (C_p) and the density (d) using $k = \alpha C_p d$ equation. For the measurement of the specific heat, a standard sample is used at room temperature to find the absorbed energy of the sample. Then, the specific heat of an unknown sample is found at a target temperature by comparing the temperature changes of the sample at room temperature and target temperature, assuming that the same heat capacity is absorbed by the unknown sample.

3 Results and discussion

XRD pattern for the microwave-solvothermally synthesized powder is shown in Fig. 1, which confirms that hexagonal (space symmetry group of $R\bar{3}m$) phase

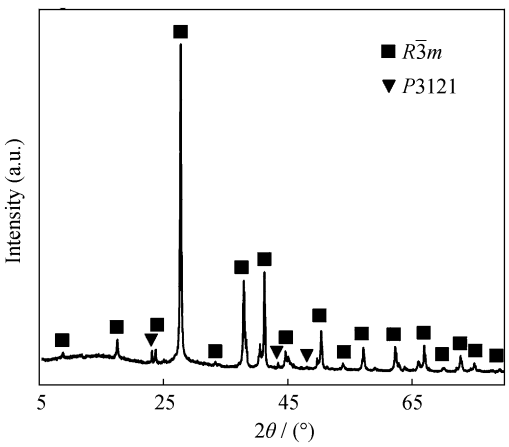

Fig. 1 XRD pattern of starting powder

characteristic for bismuth telluride is a dominant one. Besides, the Te phase (space symmetry group of $P3121$) can also be observed as traces at XRD pattern. The amount of Te phase is estimated to be less than $\sim$3 vol%. So, a single phase with Bi_2Te_3 structure cannot yet be formed after microwave–solvothermal synthesis. It is obviously that just after synthesis this phase will be depleted in Te to retain a stoichiometric composition of the starting powder. It should be noted that Lu atoms substitute for Bi site in Bi_2Te_3 compound and ionic radii of Bi and Lu are very close [9]. In this case, no Lu peaks can be found in Fig. 1.

TEM image in Fig. 2 shows a typical morphology of the microwave-solvothermally synthesized powder. It is seen that the powder mainly consists of irregularly shaped particles. In order to estimate a mean particle size, histogram of the particles size distribution was plotted. It is found that the experimental histogram can be described by a unimodal lognormal distribution. As known [30], the lognormal probability density function can be expressed as

$$F(d) = \frac{1}{\sqrt{2\pi}\sigma d}\exp\left(-\frac{(\ln d - \ln d_{\mathrm{m}})^2}{2\sigma^2}\right) \quad (1)$$

where d is the particle size, d_{m} is the mean particle size, and σ is the standard deviation of the logarithms of the particle sizes. The standard deviation is measure of the distribution width. Based on Eq. (1), d_{m} and σ values were estimated to be equal to $\sim$37 and 0.56 nm, respectively. So, the starting powder consisted of nanoparticles.

The starting powder was then used to prepare the bulk grained material. As was mentioned above, two fabrication methods were used to form various microstructures of the bulk samples. The first method is the cold isostatic pressing, and the second method (CIP sample) is the SPS process at temperatures of 653 and 683 K (SPS653 and SPS683 samples, respectively). So, three bulk grained samples with various microstructures could be fabricated.

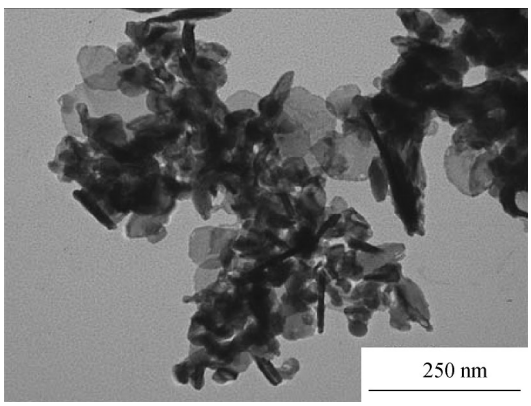

Fig. 2 TEM image of starting powder

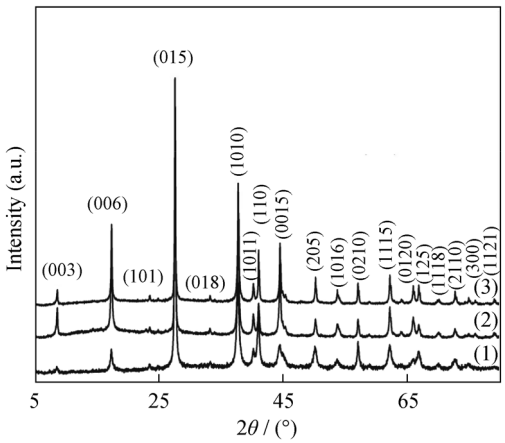

Fig. 3 XRD patterns of (1) CIP, (2) SPS653 and (3) SPS683

Figure 3 shows XRD patterns of the three samples. In contrast to the starting nanopowder, the bulk samples are single hexagonal phase with unit cell parameters of $a = b = 0.43871$ nm and $c = 3.0483$ nm. These parameters are corresponding to Bi_2Te_3 compound. It is important to note that the XRD peaks become narrower and sharper at transition from CIP to SPS653 and SPS683 samples. The peaks narrowing and sharpening can be induced by forming more perfect crystalline and grain structure depending on method and conditions of the sintering.

SEM images of a sample surface are shown in Fig. 4. One can see that microstructures of these samples are quite different and characterized by various micro-grained structures with various mean grain sizes. First of all, it should be noted that the grain growth occurs during the material fabrication. This phenomenon destroying an initial nanostructural state is characteristic for the high-temperature sintering of nanomaterials [31]. Secondly, the crystalline grained structure is not yet formed for the sample fabricated by the cold isostatic pressing (Fig. 4a). Finally, the grains have a crystal faceting for the samples fabricated by SPS method and the mean drain size increases as SPS temperature increases (Fig. 4b, c). So, the intense sintering of the starting nanopowder takes place in this case. Besides, the SPS683 sample is structurally inhomogeneous. At least, two types of the structural inhomogeneities can be observed for this sample. Figure 5a, b demonstrates the first type of these inhomogeneities. The inhomogeneities of this type are weakly compacted domains with loose structure and numerous pores in contrast to dense host material. The size of the loose domains is around a few hundreds of microns. Microcracks filled with $Bi_{1.9}Lu_{0.1}Te_3$ nanowickers are the second type of the specific structural inhomogeneities of SPS683 sample (Fig. 5c). It is very important to note that the structural inhomogeneities considered above are observed only in SPS683 sample.

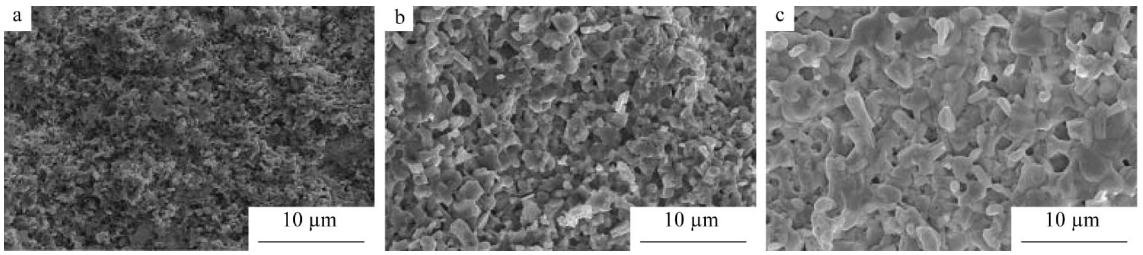

Fig. 4 SEM images of **a** CIP, **b** SPS653 and **c** SPS683

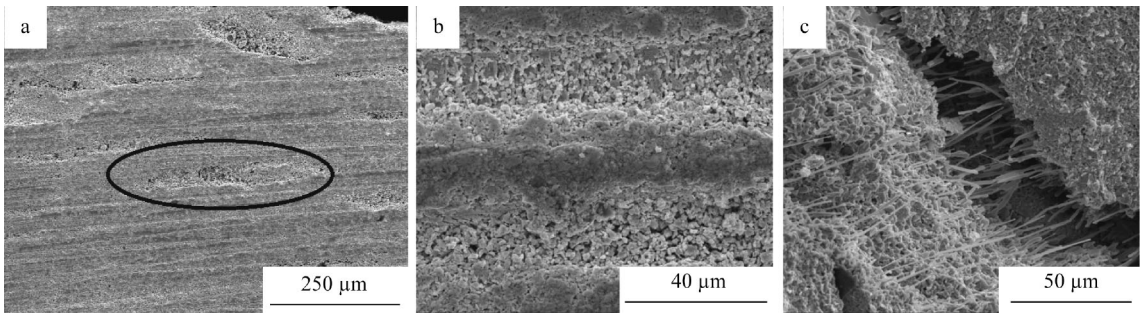

Fig. 5 SEM images of structural inhomogeneity of SPS683: **a** domains weakly compacted with loose structure, **b** detailed SEM image of domain selected in **a**, and **c** microcracks filled with $Bi_{1.9}Lu_{0.1}Te_3$ nanowickers

The samples with various microstructures have different density values. The densities of these samples are equal to 5.09, 6.06 and 5.14 $g \cdot cm^{-3}$ for CIP, SPS653 and SPS683 samples, respectively. The CIP sample with unformed crystalline grained structure has the lowest density. It is obviously that this sample still contains numerous pores formed in material during cold isostatic pressing. The temperature and time sintering after CIP process are insufficiently to form clear grained structure and increase the density. But, the SPS process allows us to prepare SPS653 and SPS683 samples with formed crystalline grained structure. The density of SPS653 sample is higher than that of CIP sample. However, the density of SPS683 sample despite the formed crystalline grained structure is close to that of CIP sample with the unformed crystalline grained structure. The structural inhomogeneities characteristic for this sample discussed above (Fig. 5) can decrease the density of SPS683 sample.

In fact, the densities of the samples under study are less than the theoretical density of Bi_2Te_3 (7.7 $g \cdot cm^{-3}$). But it should be noted that the main purpose of this paper is to find an effect of microstructure on thermoelectric properties of Lu-doped Bi_2Te_3. At present, remarkably different microstructures could be formed for samples with low density. Simultaneous optimization of the density and microstructure is next stage of our research. However, microstructural effect on thermoelectric properties of Lu-doped Bi_2Te_3 observed is reproducible. Moreover, such effect is also observed for Bi_2Te_3 compound containing other rare earth elements (Tm, Er). At present, an examination of Tm- and Er-doped Bi_2Te_3 is in progress.

In order to estimate the mean grain size of the samples with various grain structures, histograms of the grain size distributions were plotted. Diameters of more than 200 grains were measured on SEM images (Fig. 4) to obtain the reliable size distribution. The unimodal lognormal distribution was again applied to describe the experimental histograms of the grain size distributions and estimate the mean grain size (D_{gm}) and the standard deviation. The D_{gm} values are equal to $\sim$290, $\sim$730 and $\sim$1160 nm corresponding to Fig. 4a, b, c, respectively. So, the sintering of the samples is accompanied by the sufficient grain growth from the initial nanoparticles. The standard deviation of the logarithms of the particle sizes (σ) value was equal to 0.46 for all three samples with various grain structures.

Thus, a little difference of SPS temperature could surprisingly provide a remarkable change of the grain structure. It should be reminded that the initial powder for sintering consists of nanoparticles with the mean particle size of $\sim$37 nm. A considerable energy can been stored in the powder nanoparticles [32]. So, thermodynamically, such nanomaterials are far removed from their equilibrium state and a large driving force toward equilibrium exists. The stored energy is released during the heating at elevated temperatures due to the grain growth. As a consequence, grain growth will occur at elevated temperatures, leading to a concomitant increase of the grain size. The grain size increases with annealing temperature in accordance with

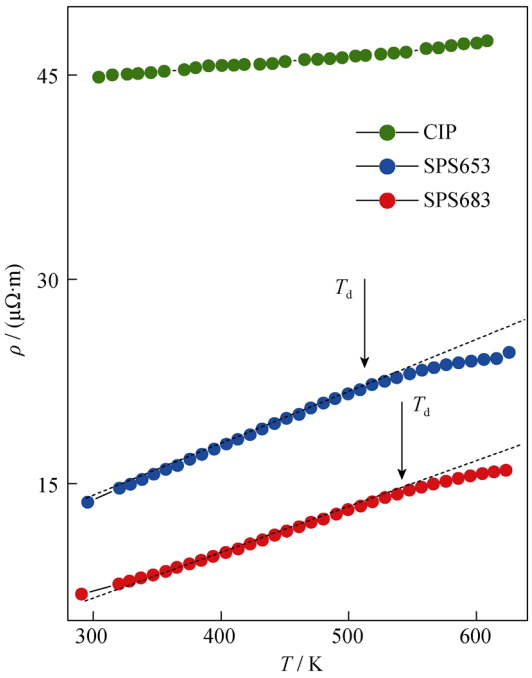

Fig. 6 Temperature dependences of specific electrical resistivity for CIP, SPS653 and SPS683

law close to an exponential growth. In this case, even a little difference of the annealing temperature will cause a significant change of the grain size. This behavior has been observed for iron [33].

The bulk $Bi_{1.9}Lu_{0.1}Te_3$ samples with various grain structures demonstrate different thermoelectric properties. Figure 6 shows temperature dependences of the specific electrical resistivity (ρ). One can see that ρ of all three samples increases as temperature increases. This behavior is typical for degenerate semiconductors and characteristic for Bi_2Te_3. The specific electrical resistivity of SPS fabricated samples is sufficiently lower than that of CIP-fabricated sample. The $\rho(T)$ dependences for SPS653 and SPS683 samples can be divided into two parts. Below some temperature (T_d), these dependences are linear. Above T_d, the experimental $\rho(T)$ curves start to deviate from linear law to lower ρ values. The T_d value is estimated as ~510 and ~540 K for SPS653 and SPS683 samples, respectively. No T_d is observed for CIP sample.

It should be noted that ρ value decreases as the mean grain size increases. It means that a contribution of grain scattering mechanism of the charge carries gradually depresses when a number of grain boundaries decreases during the grain growth at high-temperature sintering. The temperature dependence of the Seebeck coefficient (S) is shown in Fig. 7. The major charge carries in the samples under study are electrons because the Seebeck coefficients have a negative sign. As mentioned above, Lu atoms

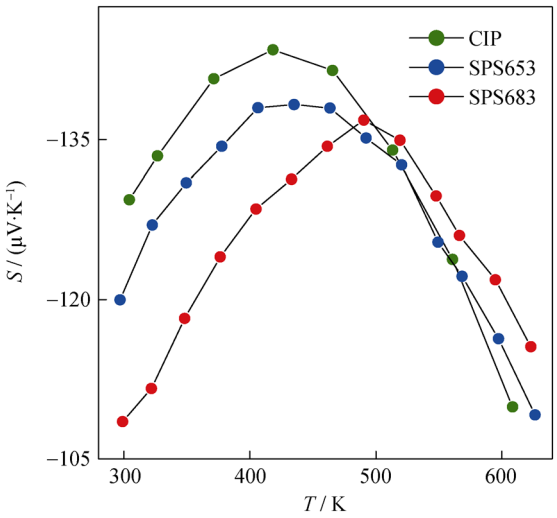

Fig. 7 Temperature dependences of Seebeck coefficient for CIP, SPS653 and SPS683

substituting for Bi site in Bi_2Te_3 compound behave as donors [9].

It is known [9] that the Seebeck coefficient of the degenerate semiconductors can be expressed as

$$S = \frac{2k_B^2 Tm^*}{3e\hbar}\left(\frac{\pi}{3n}\right)^{2/3}\left(\frac{3}{2}+\gamma\right) \quad (2)$$

where k_B is the Boltzmann's constant, n is the carrier concentration, $\hbar$ is the reduced Planck constant, m^* is the effective mass of electron, e is the charge of electron, and γ is the scattering factor. In accordance with Eq. (2), the decrease of the specific electrical resistivity is usually accompanied by the decrease of Seebeck coefficient. This behavior is in agreement with the results in Fig. 7. The amount of Lu atoms is the same for CIP, SPS653 and SPS683 samples. So, a change of the scattering factor will determine both the specific electrical resistivity and the Seebeck coefficient of these samples.

The $S(T)$ curves have maxima whose temperature position is dependent on the specific electrical resistivity of the samples with various grain structures. Such maxima are typical for Y-, Lu-, Ce-, Sm-doped Bi_2Te_3 compounds [9, 11, 12, 14, 15]. Usually, such kind of non-monotonic change of the Seebeck coefficient is attributed to a bipolar effect when two types of the charge carriers are present. Thermal excitation of the charge carriers from valence band to conduction band will generate both electrons in conduction band and holes in valence band [17]. Usually, thermal excitation does not change the concentration of the major charge carriers too much, but increases the minor carrier concentration. As mentioned above, the Seebeck coefficient of electron conductivity is negative, whereas hole conductivity is characterized by the positive Seebeck coefficient. A competition of these two contributions with

opposite signs of the Seebeck coefficient can form $S(T)$ maxima in Fig. 7. It should be noted that an appearance of $\rho(T)$ curvature at temperature T_d is in agreement with the decrease of specific electrical resistivity due to bipolar effect. The high electrical resistivity of CIP sample does not allow distinguishing the contribution of the carrier concentration change.

The temperature dependences of the power factor (S^2/ρ) are presented in Fig. 8. These dependences include the contributions from $\rho(T)$ and $S(T)$ dependences, wherein the $\rho(T)$ contribution determines the maximum S^2/ρ value and the $S(T)$ curve determines the appearance of maxima of the power factor. The maximum value of S^2/ρ is observed for the samples with low electrical resistivity fabricated by SPS method. So, the contribution of the resistivity decrease is dominant one.

The thermal conductivity (k) of the samples reveals unexpected behavior (Fig. 9). The thermal conductivity of SPS653 sample increases compared with that of CIP sample. This increase can be attributed to the grain growth, leading to the decrease of phonon and electron scattering by the grain boundaries. However, the thermal conductivity of SPS683 sample has minimum value among all three samples, although this sample is characterized by the maximum mean grain size and the lowest specific electrical resistivity. The k value of this sample is close to the thermal conductivity of Y-, Ce and Sm-doped Bi_2Te_3 compounds [11].

The k behavior of CIP, SPS653 and SPS683 samples is in contradiction with ρ change as the decrease of ρ usually leads to the increase of k. Such ρ–k relationship is stated by the Wiedemann–Franz law [17].

$$k_{\text{carr}} = L\sigma T \tag{3}$$

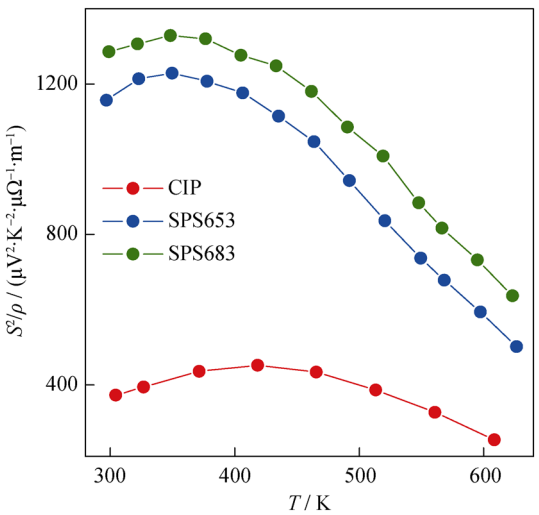

Fig. 8 Temperature dependences of power factor for CIP, SPS653 and SPS683

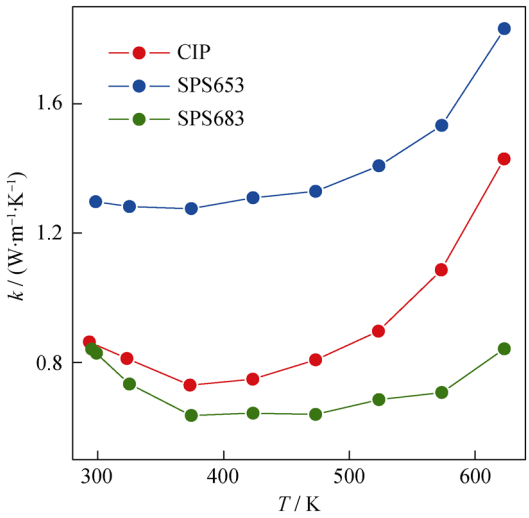

Fig. 9 Temperature dependences of thermal conductivity for CIP, SPS653 and SPS683

where k_{carr} is the charge carrier contribution to the thermal conductivity, L is the Lorenz number, and σ is the specific electrical conductivity. So, the Wiedemann–Franz law is a law for the electron thermal conductivity. In order to explain above contradiction, the lattice contribution to the thermal conductivity should be taken into account.

According to the experiments, the structural inhomogeneities (Fig. 5) can be considered as one of the main sources to decrease the thermal conductivity of SPS683 sample. First of all, the boundaries between the structural inhomogeneities and the bulk host material can additionally depress the thermal conductivity. These boundaries can scatter not only phonons but also electrons. The wavelength of electrons (λ) and mean free path for phonons (l) should be different so as to provide more reduction in the thermal conductivity than in the electrical conductivity. Usually, suitable λ/l ratio is provided for the thermoelectric nanomaterials [17]. In this experiment, nanowickers are observed as specific structural inhomogeneities in SPS683 sample. It is known [34] that due to the large surface area to volume ratio, small diameter phonon boundary scattering in nanowickers is much stronger than in bulk materials, which leads to the reduced phonon mean free path and thermal conductivity of nanowickers. For instance [17], Bi_2Te_3 composite filled with Bi_2Te_3 nanowickers demonstrates low thermal conductivity of $\sim$0.8 $W{\cdot}m^{-1}{\cdot}K^{-1}$ at room temperature while $\sim$1.2 $W{\cdot}m^{-1}{\cdot}K^{-1}$ for commercial Bi_2Te_3. Thus, SPS683 sample contains the structural inhomogeneities beneficial for the reduction of the thermal conductivity. Finally, it should be noted that simultaneous decrease of ρ and k has been observed in Lu-doped Bi_2Te_3 compound [9].

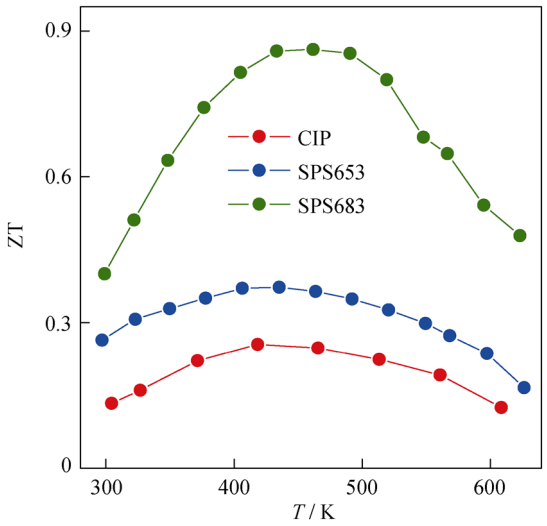

Fig. 10 Temperature dependences of figure of merit for CIP, SPS65 and SPS683

The temperature dependences of ZT are shown in Fig. 10. One can see that SPS683 sample has the highest ZT values over the whole measured temperature range, which can be attributed to the lowest specific electrical resistivity and thermal conductivity. The maximum ZT value is equal to ~0.9 for the temperature range of 450–500 K.

4 Conclusion

The bulk $Bi_{1.9}Lu_{0.1}Te_3$ samples with various micro-grained structures were fabricated by cold isostatic pressing and SPS. It is found that the mean grain size is equal to ~290, ~730 and ~1160 nm for CIP and SPS at 653 and 683 K samples, respectively. The micro-grained sample with maximum mean grain size shows the lowest specific electrical resistivity and thermal conductivity and the maximum dimensionless figure of merit (ZT ≈ 0.9 for the temperature range of 450–500 K).

Acknowledgements This work was financially supported by the Ministry of Education and Science of the Russian Federation (No. 3.6586.2017/BY and 03.G25.31.0246).

References

[1] Mahan G, Sales B, Sharp J. Thermoelectric materials: new approaches to an old problem. Phys Today. 1997;50(3):42.
[2] Tritt TM. Thermoelectric materials: holey and unholey semiconductors. Science. 1999;283(5403):804.
[3] Lan YC, Minnich AJ, Chen G, Ren ZF. Enhancement of thermoelectric figure-of-merit by a bulk nanostructuring approach. Adv Funct Mater. 2010;20(3):357.
[4] Snyder GJ, Toberer ES. Complex thermoelectric materials. Nat Mater. 2008;7(2):105.
[5] Kitagawa H, Nagamori T, Tatsuta T, Kitamura T, Shinohara Y, Noda Y. Liquid phase growth of $Bi_{0.5}Sb_{1.5}Te_3$ by sliding-boat method. Scr Mater. 2003;49(4):309.
[6] Hyun DB, Oh TS, Hwang JS, Shim JD, Kolomoets NV. Electrical and thermoelectric properties of 90% Bi_2Te_3-5% Sb_2Te_3-5% Sb_2Se_3 single crystals doped with SbI_3. Scr Mater. 1998;40(1):49.
[7] Miura S, Satob Y, Fukuda K, Nishimura K, Ikeda K. Texture and thermoelectric properties of hot-extruded Bi_2Te_3 compound. Mater Sci Eng A. 2000;277(1–2):244.
[8] Ivanov O, Maradudina O, Lyubushkin R. Preparation and characterization of bulk composite constructed of Bi_2Te_3@SiO_2 nanoparticles. J Alloys Compd. 2014;586:679.
[9] Yang J, Wu F, Zhu Z, Yao L, Song H, Hu X. Thermoelectrical properties of lutetium-doped Bi_2Te_3 bulk samples prepared from flower-like nanopowders. J Alloys Compd. 2015;619:401.
[10] Ji XH, Zhao XB, Zhang YH, Lu BH, Ni HL. Synthesis and properties of rare earth containing Bi_2Te_3 based thermoelectric alloys. J Alloys Compd. 2005;387(1–2):282.
[11] Wu F, Song H, Jia J, Hu X. Effect of Ce, Y and Sm on the thermoelectric properties of Bi_2Te_3 alloy. Prog Nat Sci Mater Int. 2013;23(4):408.
[12] Wu F, Shi W, Hu X. Preparation and thermoelectric properties of flower-like nanoparticles of Ce-doped Bi_2Te_3. Electron Mater Lett. 2015;11(1):127.
[13] Ji XH, Zhao XB, Zhang YH, Lu BH, Ni HL. Solvothermal synthesis and thermoelectric properties of lanthanum contained Bi–Te and Bi–Se–Te alloys. Mater Lett. 2005;59(6):682.
[14] Wu F, Song HZ, Jia JF, Gao F, Zhang YJ, Hu X. Thermoelectric properties of Ce-doped n-type $Ce_xBi_{2-x}Te_{2.7}Se_{0.3}$ nanocomposites. Phys Status Solidi A. 2013;210(6):1183.
[15] Shi WY, Wu F, Wang KL, Yang JJ, Song HZ, Hu X. Preparation and thermoelectric properties of yttrium-doped Bi_2Te_3 flower--like nanopowders. J Electron Mater. 2014;43(9):3162.
[16] Zhao XB, Zhang YH, Ji XH. Solvothermal synthesis of nano--sized $La_xBi_{(2-x)}Te_3$ thermoelectric powders. Inorg Chem Commun. 2004;7(3):386.
[17] Liu W, Yan X, Chen G, Ren Z. Recent advances in thermoelectric nanocomposites. Nano Energy. 2012;1(1):42.
[18] Li Y, Jiang J, Xu G, Li W, Zhou L, Li Y, Cui P. Synthesis and micro/nanostructured p-type $Bi_{0.4}Sb_{1.6}Te_3$ and its thermoelectrical properties. J Alloys Compd. 2009;480(2):954.
[19] Kim SS, Yamamoto S, Aizawa T. Thermoelectric properties of anisotropy-controlled p-type Bi–Te–Sb system via bulk mechanical alloying and shear extrusion. J Alloys Compd. 2004;375(1–2):107.
[20] Morisaki Y, Araki H, Kitagawa H, Orihashi M, Hasezaki K, Kimura K. Bi_2Te_3-related thermoelectric samples with aligned-texture prepared by plastic deformation. Mater Trans. 2005;46(11):2518.
[21] Duan X-K, Hu K-G, Ma D-H, Zhang W-N, Jiang Y-Z, Guo S-C. Microstructure and thermoelectric properties of $Bi_{0.5}Na_{0.02}Sb_{1.482-x}In_xTe_3$ alloys fabricated by vacuum melting and hot pressing. Rare Met. 2015;34(11):770.
[22] Ivanov O, Maradudina O, Lyubushkin R. Grain size effect on electrical resistivity of bulk nanograined Bi_2Te_3 material. Mater Charact. 2015;99:175.
[23] Lee SM, Cahill DG, Venkatasubramanian R. Thermal conductivity of Si–Ge superlattices. Appl Phys Lett. 1997;70(22):2957.
[24] Vining CB, Laskow W, Hanson JO, Van der Berk RR, Gorsuch PD. Thermoelectric properties of pressure-sintered $Si_{0.8}Ge_{0.2}$ thermoelectric alloys. J Appl Phys. 1991;69(8):4333.
[25] Zhang Q, Che S, Liu W, Lukas K, Yan X. Suppression of grain growth by additive in nanostructured p-type bismuth antimony tellurides. Nano Energy. 2012;1(1):183.

[26] Ji X, He J, Alboni P, Su Z, Gothard N, Zhang B, Tritt TM, Kolis JW. Thermal conductivity of $CoSb_3$ nano-composites grown via a novel solvothermal nano-plating technique. Phys Status Solidi RRL. 2007;1(6):229.
[27] Zhang Q, He J, Zhu TJ, Zhang SN, Zhao XB, Tritt TM. High figures of merit and natural nanostructures in $Mg_2Si_{0.4}Sn_{0.6}$ based thermoelectric materials. Appl Phys Lett. 2008;93(10): 102109.
[28] Deng Y, Zhou XS, Wei GD, Liu J, Nan CW, Zhao SJ. Solvothermal preparation and characterization of nanocrystalline Bi_2Te_3 powder with different morphology. J Phys Chem Solids. 2002;63(11):2119.
[29] Zhao XB, Ji XH, Zhang YH, Lu BH. Effect of solvent on the microstructures of nanostructured Bi_2Te_3 prepared by solvothermal synthesis. J Alloys Compd. 2004;368(1–2):349.
[30] Humphreys FJ, Hatherly M. Recrystallization and Related Annealing Phenomena. Oxford: Elsevier; 2004. 520.
[31] Scheele M, Oeschler N, Meier K, Kornowski A, Klinke C, Weller H. Synthesis and thermoelectric characterization of Bi_2Te_3 nanoparticles. Adv Funct Mater. 2009;19(21):3476.
[32] Groza JR. Non-Equilibrium Processing of Materials. In: Suryanarayana C, editor. Science. Oxford: Elsevier; 1999. 47.
[33] Moelle CH, Fecht HJ. Thermal stability of nanocrystalline iron prepared by mechanical attrition. Nanostruct Mater. 1995; 6(1–4):421.
[34] Hochbaum AI, Chen R, Delgado RD, Liang W, Garnett EC, Najarian M, Majumdar R, Yang P. Enhanced thermoelectric performance of rough silicon nanowires. Nature. 2008; 451(7175):163.